

## DOCUMENT CONTROL DATA - R &amp; D

(Security classification of title, body of abstract and indexing annotation must be entered when the overall report is classified)

1. ORIGINATING ACTIVITY (Corporate author) Naval Research Laboratory Washington, D. C. 20390		2a. REPORT SECURITY CLASSIFICATION Unclassified	
		2b. GROUP	
3. REPORT TITLE  TRANSIENT RADIATION EFFECTS ON RUBY LASERS			
4. DESCRIPTIVE NOTES (Type of report and inclusive dates) Final Report on a continuing problem.			
5. AUTHOR(S) (First name, middle initial, last name) Richard F. Wenzel Joseph J. Halpin Francis J. Campbell			
6. REPORT DATE February 20, 1970		7a. TOTAL NO. OF PAGES 96	7b. NO. OF REFS 34
8a. CONTRACT OR GRANT NO. DASA RAEV TA 028		9a. ORIGINATOR'S REPORT NUMBER(S)  NRL Report 7063	
b. PROJECT NO. NRL 64E02-05		9b. OTHER REPORT NO(S) (Any other numbers that may be assigned this report)	
c.			
d.			
10. DISTRIBUTION STATEMENT This document has been approved for public release and sale; its distribution is unlimited.			
11. SUPPLEMENTARY NOTES		12. SPONSORING MILITARY ACTIVITY Defense Atomic Support Agency 473 T Building Washington, D. C. 20305	
13. ABSTRACT This technical report describes ionizing radiation effects on a ruby laser. Both transient and permanent radiation effects are discussed. The transient cut-off observed in a ruby laser when irradiated is attributed to a transient optical absorption center associated with a $O^-$ ion trapped at a charge deficient cation site in the $Al_2O_3$ lattice. The center has a lifetime of about 10 msec at room temperature. The permanent radiation effects are a reduction of or cessation of laser output. This effect has three causes, color center formation in the pump bands, loss of $Cr^{3+}$ by valence change, and a permanent absorption at the R lines. The important effect at the level of $1 \times 10^4$ rad (ruby) is color center formation in the pump bands. A worse case estimate is, ignoring flash lamp bleaching, for a 0.05% $Cr^{3+}$ , 0.25 inch. diam. rod of $60^\circ$ orientation, (a typical ruby laser rod), that a dose of $1 \times 10^4$ rad (ruby) will reduce the optical pumping by 10%. This means that $1 \times 10^4$ rad (ruby) will shut off a laser operating at 110% threshold.  The defects producing the color centers are isolated, remotely charge compensated defects in the lattice. Locally charge compensated defects which involve a $Cr^{3+}$ ion are also observed and account for most of the $Cr^{3+}$ loss on irradiation. The maximum $Cr^{3+}$ loss observed, independent of concentration was 10%.			

## CONTENTS

	Page
I. INTRODUCTION	1
II. PRELIMINARY INVESTIGATIONS	3
Flash Lamp Vulnerability	6
Radiation Sensitivity of Coupling Reflector	9
Radiation Sensitivity of the End Mirrors	9
III. TRANSIENT DAMAGE MECHANISM	11
Two Rod Experiment	11
Transient Optical Absorption Measurement	13
Chromium as a "Getter"	22
Low Temperature Optical Absorption	23
Conclusions on Transient Absorption Effect	26
IV. PERMANENT DAMAGE MECHANISM	28
Permanent Color Centers at the R Line	28
Relative Fluorescent Experiment	30
Ruby Rangefinder Experiments	35
Bleaching Kinetics and Band Resolution	37
Kinetic Studies	50
Electron Paramagnetic Resonance Studies	58
Defect Model	73
Increase in Ruby Laser Output by $^{60}\text{Co}$ Irradiation	79
Ruby Laser Damage Calculation at $1 \times 10^4$ rads (ruby)	80
V. SUMMARY	87
REFERENCES	90

# TRANSIENT RADIATION EFFECTS ON RUBY LASERS

## I. INTRODUCTION

The program of transient nuclear radiation effects on lasers was initiated in early 1966 with a survey of military applications for laser devices. The aim was to determine which laser systems would have hardness requirements and to establish a priority of research effort among these, based upon the imminence of field readiness. The survey also probed for estimates of probable exposures in the most vulnerable applications and for the critical elements of the systems at these levels.

Briefly, the survey found that military applications utilize all three of the basic laser types - solid state, gas, and semiconductor. These applications include ranging (on tanks, artillery, ships, and aircraft), target illumination, target recognition, missile guidance, proximity fuzing, secure communications, radar, field computer links, laser gyro, navigation aids, and underwater detection of submarines, mines, and submerged obstacles.

The results of this survey indicated that several laser devices were in the advanced development stage and were to be used in applications where radiation requirements existed. Of these, the Army had ordered field test units of several ruby rangefinders. Also, it was determined that several other systems employing neodymium (Nd) lasers would soon be in use. Since that time, these ruby rangefinders and several Nd devices have gone into production.

## II. PRELIMINARY INVESTIGATIONS

The vulnerability of the ruby laser to pulsed ionizing radiation was demonstrated in an irradiation experiment similar to that employed by D. M. J. Compton.<sup>3,4</sup> A ruby laser (Optics Technology Model 120) was modified by cutting slits in the lamp reflector so that the laser rod could be irradiated directly. The laser was operated in the "long pulse" mode in which case it emits a 0.7 msec train of pulses of coherent light (pulse width of approximately 0.4  $\mu$ sec) with an average time interval between the pulses of 5 to 10  $\mu$ sec. The amplitude of the pulse is also random. During the train of pulses, a 1 cm portion of the ruby rod was irradiated with 30 MeV electrons from a LINAC (100 ma, 0.5  $\mu$ sec pulse).

Figure 1 shows the effect of the irradiation on the laser output. In this case the lasing stops for about 50  $\mu$ sec. This indicates that the radiation has produced a transient damage mechanism. When the pulsed output energy is measured before and after irradiation at constant pumping level, it is found that the output has decreased substantially, revealing in addition the existence of permanent damage.

Figure 2 shows a reduction<sup>\*</sup> in output power of a ruby laser exposed to  $3.6 \times 10^4$  rad (ruby) delivered by 30 MeV electrons. The irradiation reduced the energy output to 60% of its pre-irradiation value for the first laser pulse after the irradiation.

---

<sup>\*</sup>Other experimenters have also observed increases in laser output when the laser was irradiated with ionizing radiation. This occurs only when the laser is optically pumped at several times the threshold for laser action. All military ruby laser systems employ pumping levels considerably lower than this. Some new information on this effect is discussed on page 79.

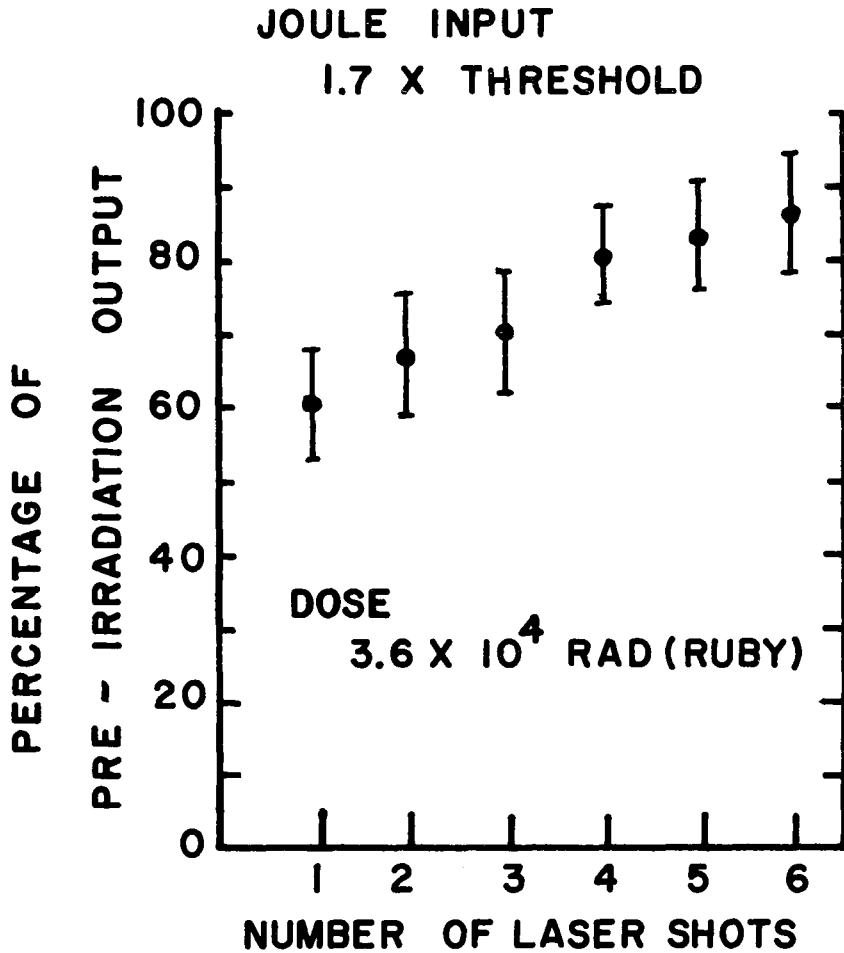


Fig. 2

LASER POWER OUTPUT AFTER A SINGLE IRRADIATION PULSE  
 VERSUS NUMBER OF LASER SHOTS

The change in the output of a ruby laser, measured as the percentage of the pre-irradiation output after a dose of  $3.6 \times 10^4$  rad (ruby).

The laser was operated at 1.7 times threshold.

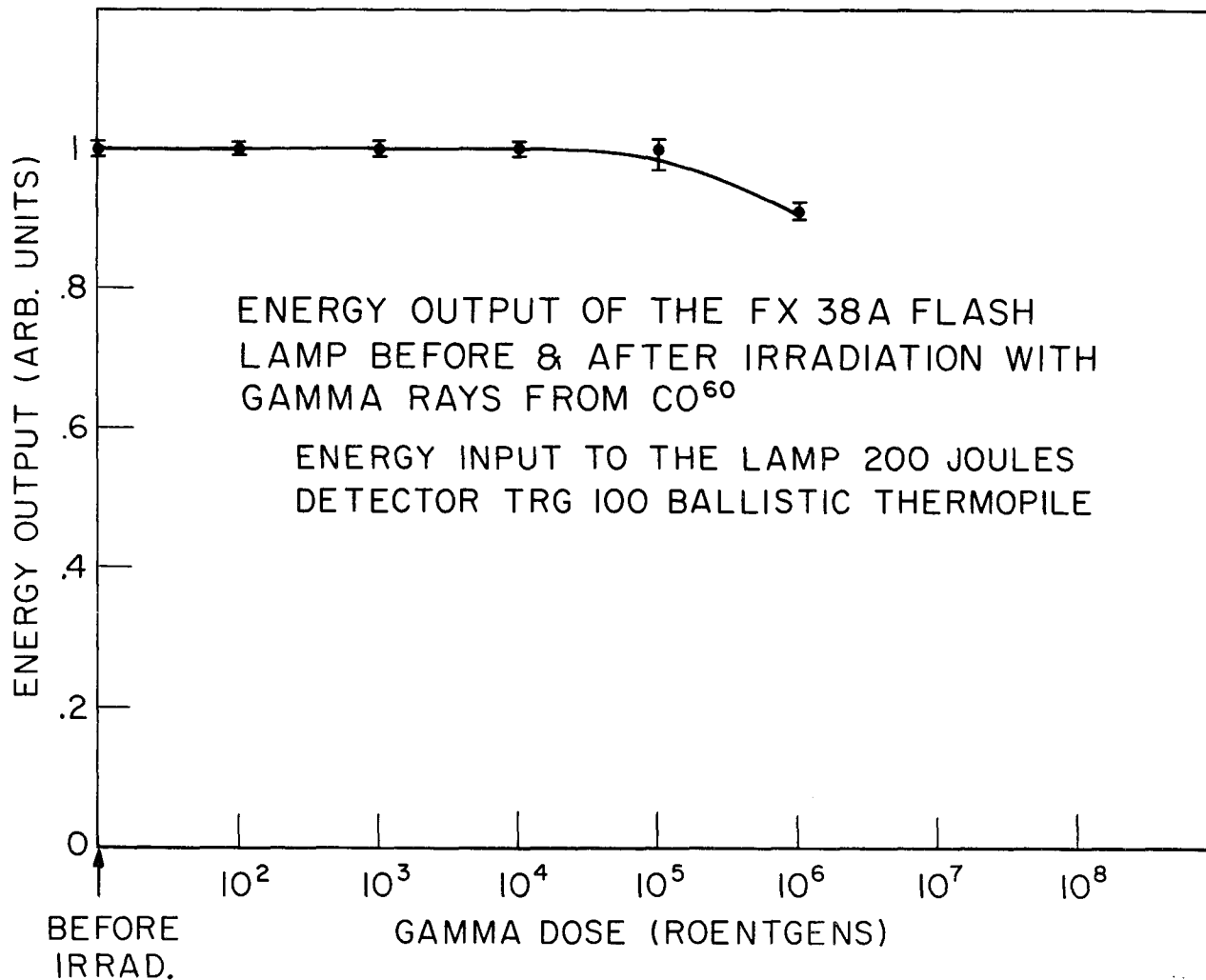


Fig. 3

ENERGY OUTPUT OF FX 38A FLASH LAMP VERSUS EXPOSURE

### Radiation Sensitivity of Coupling Reflector

Several types of reflectors are commonly used in a ruby laser. When the coupling reflector is made from a highly polished aluminum surface or aluminum coated with some highly reflecting film (e. g. nickel) there are no damaging effects produced by ionizing radiation up to  $10^6$  rad (aluminum). If the reflector substrate is a transparent material, typically glass, with a reflecting film (e. g. silver) on the outside (i. e. , a back surface mirror) there can be a damaging effect. The damage would be a loss of efficiency of the reflector by the creation of color centers in the transparent media. This problem can be solved by the use of radiation resistant transparent materials such as synthetic sapphire, high purity synthetic fused silica, or cerium-doped glass.

### Radiation Sensitivity of the End Mirrors

The standard high power dielectric mirrors on fused silica substrates have withstood electron irradiations and reactor irradiations up to the exposures of interest and were not considered in this work.<sup>5</sup> However, the vulnerability of prisms would be dependent on their composition. The same would be true of metallic reflectors evaporated on a substrate, i. e. , no damage is expected in the film; however, the substrate vulnerability is dependent on its composition.

It should be pointed out that if deflecting or focusing optics are used in a laser system, the vulnerability of these elements to coloration should be known.

### III. TRANSIENT DAMAGE MECHANISM

#### Two Rod Experiment

The temporary interruption of lasing by ionizing radiation was investigated by constructing a laser cavity which contained two rods, either of which could be irradiated.<sup>6</sup> A diagram of this experiment is shown in Fig. 4. The ruby laser is in the same configuration as was used in the previous experiment. However, in this case a rod of pure sapphire ( $\text{Al}_2\text{O}_3$ ), which is the host crystal lattice for the chromium ion in ruby ( $\text{Al}_2\text{O}_3:\text{Cr}$ ), has also been inserted in the cavity. The sapphire was shielded so that it was not illuminated by the flash lamp which pumps the laser. The optical loss associated with the insertion of this rod is small, as the sapphire rod had an antireflective coating on the ends, resulting in negligible reflection losses at the lasing wavelength before and after the irradiation. Both of the rods were made by Linde by the Czochralski process. Either rod could be irradiated by 30 MeV electrons from a LINAC. The end coatings on both rods were not affected by the irradiation.

When the ruby rod alone was irradiated, the laser behaved as was observed previously. However, when the sapphire rod alone was irradiated at the same dose level, the transient cut-off was much longer (by a factor of ten). The increased radiation sensitivity of the  $\text{Al}_2\text{O}_3$  rod, fabricated in the same size and shape, and by the same growth method as the ruby rod, points to a single defect mechanism which is more effective in the sapphire rod than in the ruby rod. The chromium in the ruby appears to suppress the damage mechanism.

The cut-off time (time that the laser is off) as a function of dose is shown in Fig. 5. The cut-off time is seen to saturate at about  $2 \times 10^4$  rad, (ruby).

The damage mechanism which this experiment suggested was the formation of transient optical absorption at the lasing wavelength. The introduction of even a small additional optical absorption of laser light in the cavity would cause a cessation of lasing. The resumption of laser action would then be due to the laser increasing the level of coherent light inside the cavity so as to make up for the additional loss, or by the optical absorption having a short time constant and thus rapidly dying away.

Transient optical absorption would be caused by defect centers in the ruby/sapphire lattice which, while normally not capable of absorbing light, can momentarily trap electrons or holes produced by the irradiation, to form a light absorbing color center. While this center exists, it absorbs light over a definite wavelength range which is characteristic of the particular defect. Subsequently, thermal motion releases the trapped electron or hole and the optical absorption disappears. Traps of this type may be made stable if the experiment is performed at a lower temperature. An experimental investigation of this effect is described on page 23.

#### Transient Optical Absorption Measurement

Transient color centers were the most likely defect mechanism, and a spectrometer system for measuring transient optical absorption was constructed. A schematic of this apparatus is shown in Fig. 6.

# APPARATUS SCHEMATIC

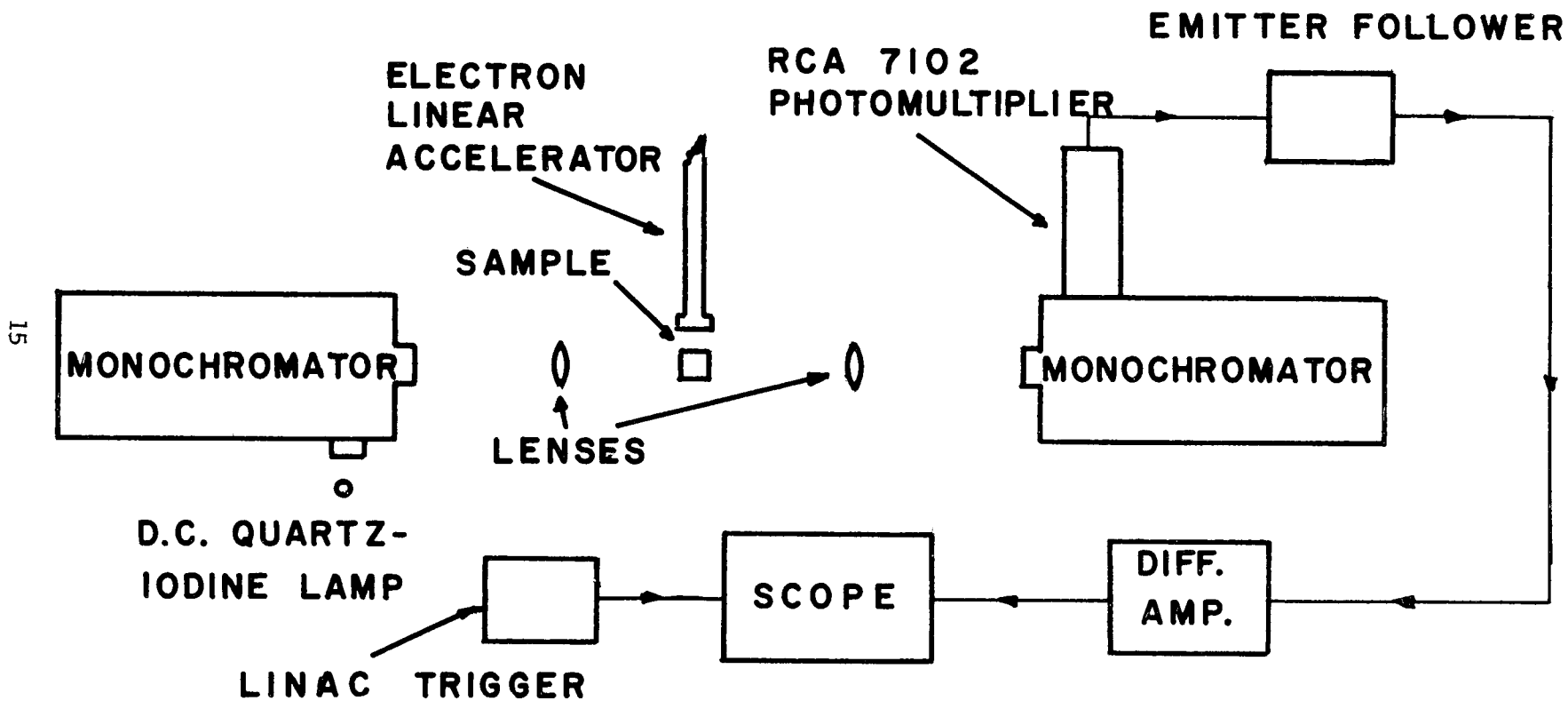


Fig. 6

TRANSIENT OPTICAL ABSORPTION SCHEMATIC

4400 Å  
SAPPHIRE

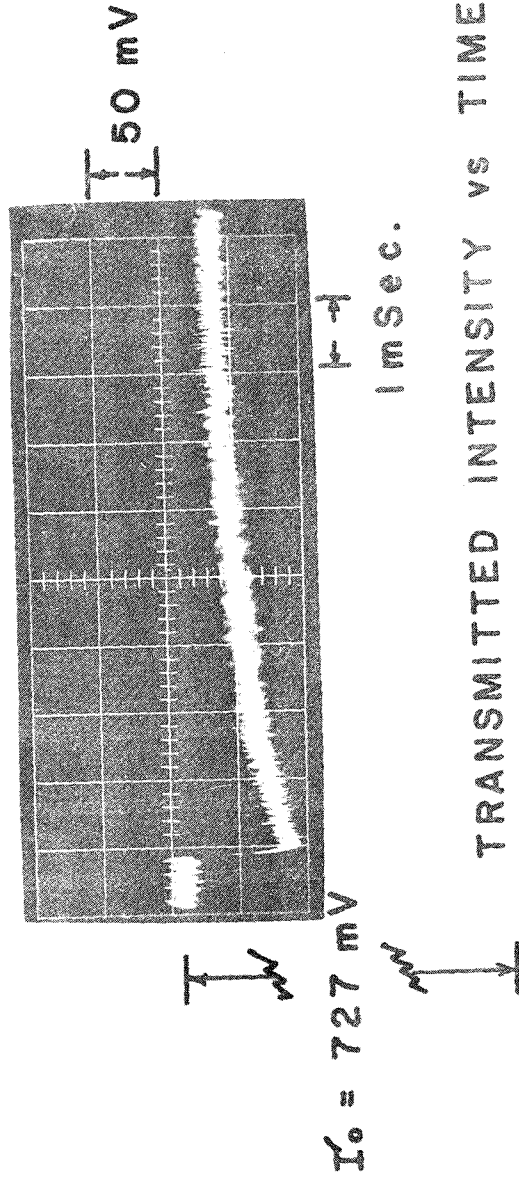


Fig. 7

TRANSIENT OPTICAL ABSORPTION IN SAPPHIRE

The transient optical absorption at 4400 Å in sapphire, versus time. The baseline has been offset 727 mV. The Linac fires at approximately 1 msec.

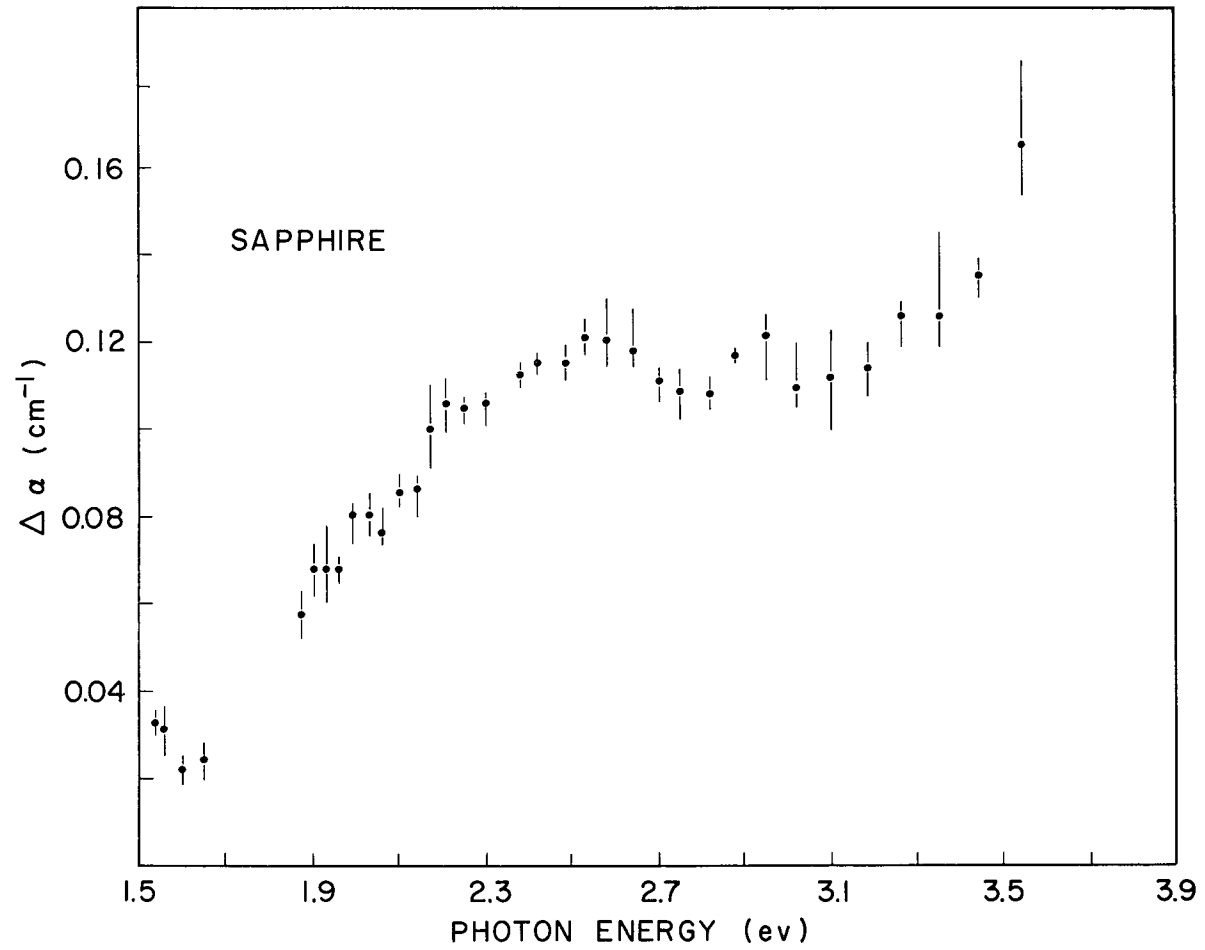


Fig. 8  
TRANSIENT ABSORPTION COEFFICIENT VERSUS  
PHOTON ENERGY FOR SAPPHIRE AT 1 MSEC  
Absorption coefficient at a constant dose of  $2 \times 10^4$  rad (ruby).

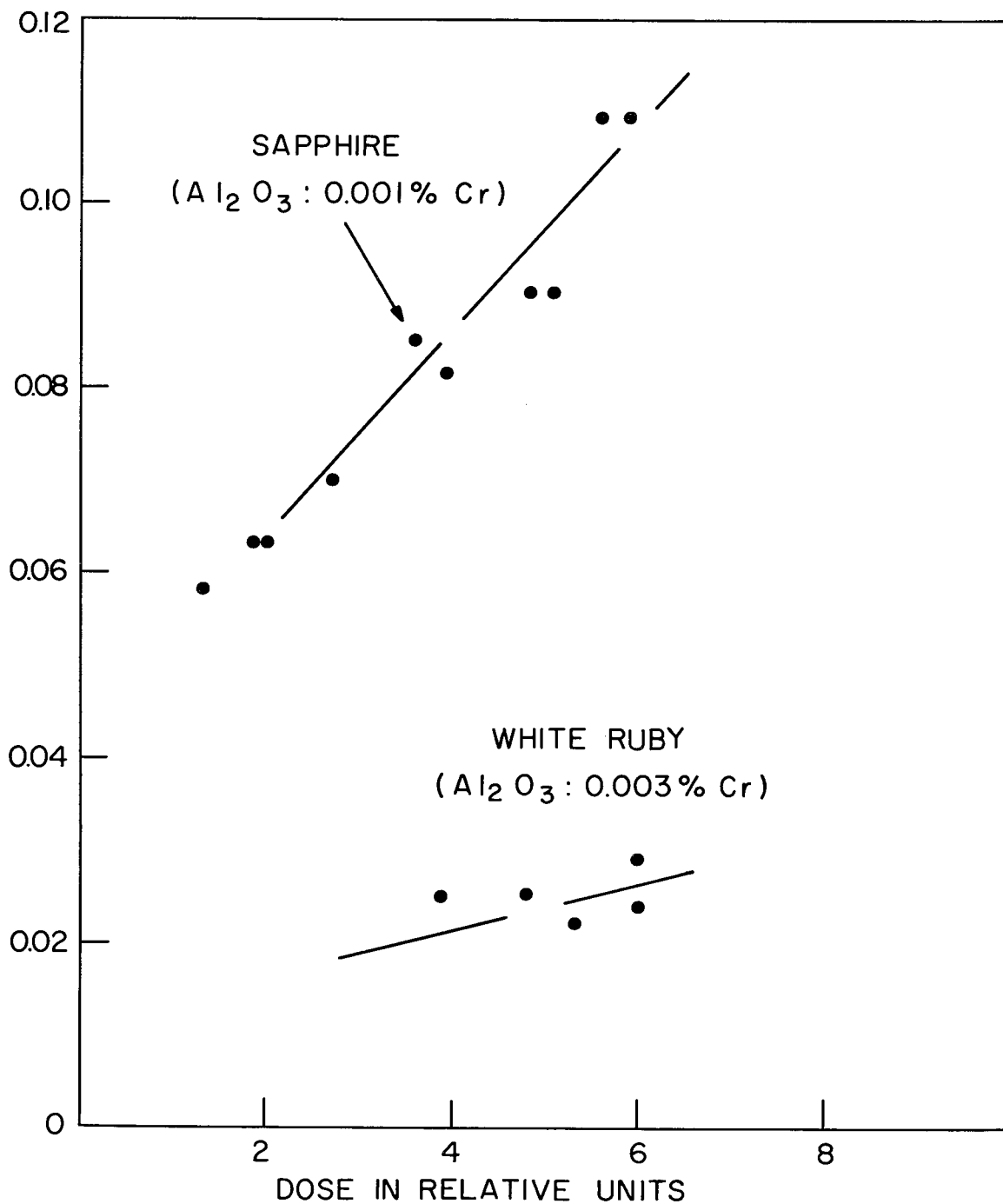


Fig. 9

TRANSIENT ABSORPTION COEFFICIENT AT 6500 Å

The transient absorption coefficient, taken 1 msec after the linac pulse in 0.001 and 0.003 percent Cr samples. The ordinate is in units of the absorption coefficient (cm<sup>-1</sup>).

The mechanism for the fluorescence produced by radiation is that an electron and a hole have recombined at the  $\text{Cr}^{3+}$  site, leaving the  $\text{Cr}^{3+}$  ion in an optically excited state. The  $\text{Cr}^{3+}$  returns to the ground state by emitting the characteristic R line fluorescence.

It appears also that the preferential electron/hole recombination at a chromium site is not limited to ruby. Derr<sup>7</sup> has observed reduction of the cut-off time when Cr is added to a YAG:Nd laser rod. In this case, the Cr once again prevents the formation of the centers responsible for the cut-off, this time at  $1.06 \mu$  (lasing wavelength in Nd material).

This "gettering" property of  $\text{Cr}^{3+}$  may be useful in other applications. Chromium has been successfully incorporated in  $\text{SiO}_2$  layers in MOS devices,<sup>8</sup> and the effect is the reduction of surface state formation, and also possibly, some reduction in trapped charged density. The mechanism currently held responsible for this effect is a structural firming of the amorphous  $\text{SiO}_2$ . The chromium fills some of the voids in the  $\text{SiO}_2$  structure and inhibits contraction of the lattice under irradiation. However, Cr in  $\text{SiO}_2$  may also have the effect of recombining radiation-produced electrons and holes thus preventing the filling of deep surface traps, and also reducing the traps in the bulk of the  $\text{SiO}_2$ . It thus may be possible, in insulators to incorporate "getter" ions, such as chromium, to reduce space charge effects.

#### Low Temperature Optical Absorption

The transient coloration of sapphire has a relatively long life-time

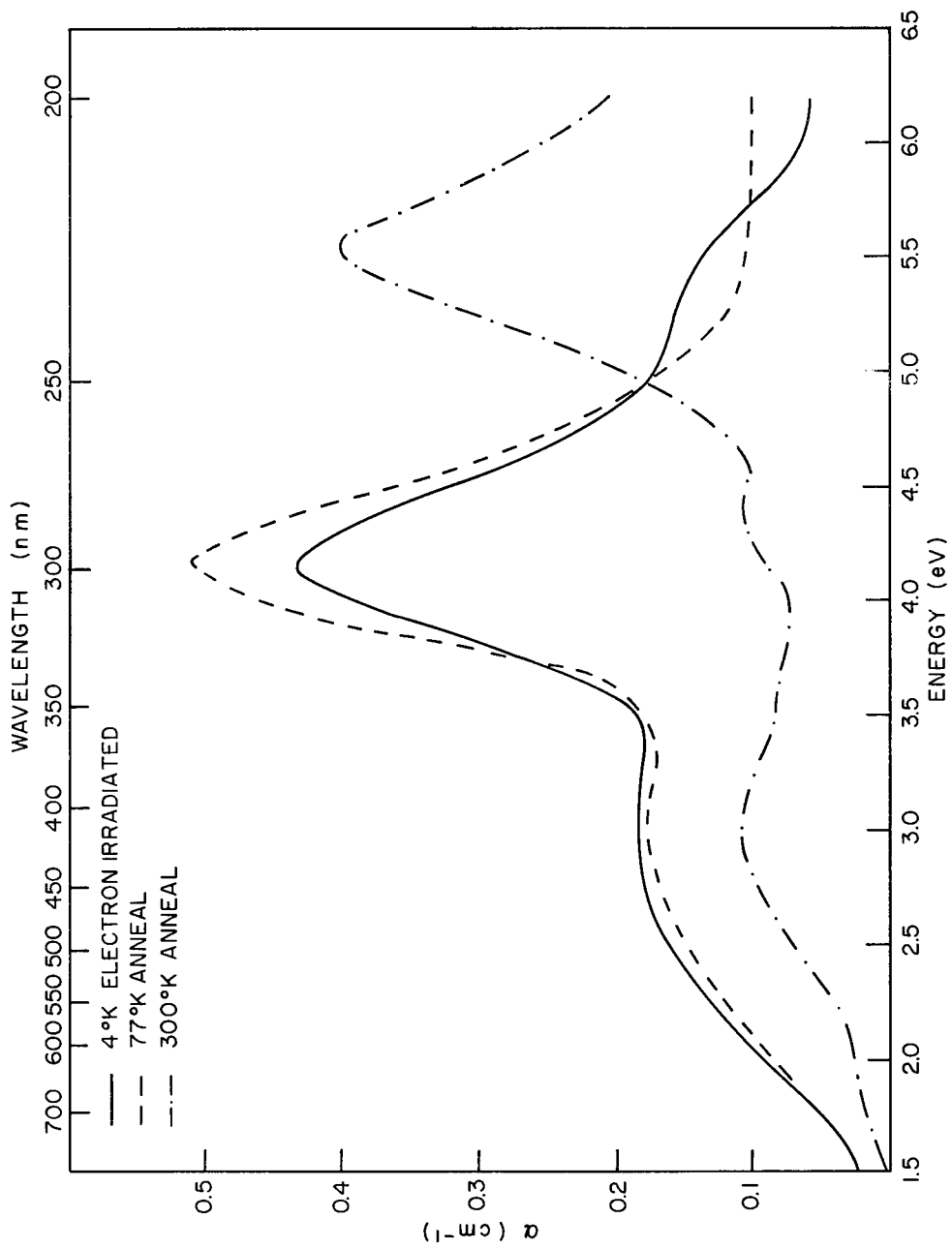


Fig. 10

INDUCED ABSORPTION IN SAPPHIRE AT LOW TEMPERATURE

color center lifetime is moderately short (10 msec.). Since most current military ruby lasers are of this type, an effort to reduce the cut-off would not be very rewarding. This work on the transient effects in ruby is therefore considered to be a sufficient treatment of the subject. However, the cut-off effect is of prime importance in nuclear pumped lasers<sup>7</sup> where the laser is subjected to continual irradiation.

the color centers. The optical absorption coefficient of these samples near the R line was measured by a spectrophotometer. The samples were then optically bleached by a mercury arc while inside the spectrophotometer chamber without disturbing the orientation of the crystals. The absorption coefficients of the crystals were again measured. The resulting absorption coefficients due to the irradiation are given in Table I.

TABLE I

Sample Number	Absorption Coefficient Near 6943Å for $1 \times 10^6$ rad (ruby)	
	Cr Concentration*	$\alpha$ ( $\text{Cm}^{-1}$ )
1	~ 0.001 CZ	0.0125
2	0.001 V	0.009
3	0.010 CZ	0.010
4	0.026 V	0.018
5	0.05 CZ	0.019
6	0.10 V	0.024

The optical absorption coefficient of about  $0.01 \text{ cm}^{-1}$  near 6943 Å is in agreement with the value typically found in pure sapphire. The variations found in Samples 1 through 3 are within reason, as this color center band has been observed to vary somewhat in saturated strength.<sup>9</sup>

\*CZ indicates Czochralski growth, V indicates Verneuil.

The ruby laser is excited by shining light into two broad absorption bands (pump bands, 25,000 and 18,000  $\text{cm}^{-1}$ ) of the  $\text{Cr}^{3+}$  ion. The energy level diagram for the optical levels of  $\text{Cr}^{3+}$  in  $\text{Al}_2\text{O}_3$  is shown in Fig. 11. The ion quickly decays (non-radiatively) to the metastable R levels (14,448 and 14,419  $\text{cm}^{-1}$ ) and subsequently returns to the ground state through R line fluorescence, or by the lasing process. The color center bands in the pump region enhance the fluorescence at the R line for pumping levels of several times threshold, but decrease the fluorescence by absorbing pump light for pumping levels below twice threshold. Military lasers operate below twice threshold. The enhancement effect will be discussed on page 79.

The radiation induced color centers were demonstrated to be detrimental to laser action at low light intensities by a relative fluorescent experiment. The monochromatic light from a Cary 14 spectrophotometer was shone on a ruby sample (0.05%  $\text{Cr}^{3+}$ ) and the fluorescence at the R line was measured with a RCA 7102 photomultiplier, equipped with two optical filters which passed only the R line light, placed at right angles to the exciting beam. The photomultiplier was connected to the pen drive amplifier of the Cary 14 through a 100 K ohm load resistor. As the wavelength of the exciting light was varied, the chart recorder of the Cary 14 recorded the variation in R line fluorescent intensity.

In performing this experiment, full advantage was again taken of a fact which greatly simplified and improved the measurement. It is known

that an ultraviolet light will bleach the color centers (see page 45 ). Unfiltered light from a 230 watt (Hanovia, Model 2223) mercury lamp will bleach the color centers in a few minutes. This optical bleaching returns the ruby sample to its pre-irradiation state. The irradiation experiments could consequently be done in reverse order. The irradiated relative fluorescent intensity was taken first, then the crystal was optically bleached to remove the color centers. The unirradiated fluorescent intensity could then be taken without having to reposition the sample.

The fluorescence at the R line can be observed as a function of the wavelength of the exciting light before and after irradiation. Although the absolute intensity of the fluorescence is not known, only the relative values before and after irradiation are important. This relative fluorescence measurement is independent of photomultiplier sensitivity and excitation light spectral intensity. The optical absorption overlapping the R line, discussed in the preceding section, is so small that it can be neglected. The data is reported in Fig. 12 as the percentage efficiency after irradiation. An efficiency of 90% means only 90% of the post-irradiation exciting light at the wavelength in question was effective for exciting R line fluorescence. Two curves are shown for an exposure of  $1.7 \times 10^3$  rads (ruby) and  $1 \times 10^6$  rads in a  $^{60}\text{Co}$  gamma ray source. At both levels the influence of the color centers is shown to be detrimental to the excitation of the R line fluorescence and hence detrimental to the operation of a laser.

This result is in contrast to work by Arkhangelskii et al.<sup>13</sup>, who calculated an increase of about 25% in the fluorescence at the R line after irradiation due to the light absorbed by the color center bands. Their work, however, does not appear to take properly into account the absorption of the  $\text{Cr}^{3+}$  ions. The "active bands" which they mention as contributing to the R line fluorescence appear to fall just at the position of the normal ruby pump bands.

### Ruby Rangefinder Experiments

As a practical evaluation of the effect of the radiation induced permanent color centers on a military laser system, a cooperative experiment was performed with Frankford Arsenal. Frankford Arsenal was responsible for the research and development of several Army portable ruby rangefinders.

The rangefinder studied utilized a Q-switched laser with a nominal output of about 3 megawatts. It was not designed to be radiation hardened and experiments performed on it are only meant to be representative.

This rangefinder was designed to operate just above threshold (107% threshold). Threshold is a term used to describe the condition where the laser will just operate with negligible output. This means that if 7% or more optical losses are sustained, the laser will not operate.

A prototype rangefinder was put through standard output tests at Frankford Arsenal by their staff. The ruby rod was removed and shipped to NRL where the rod was irradiated in the  $^{60}\text{Co}$  facility to an exposure of  $1 \times 10^6$  R. [approximately  $1 \times 10^6$  rad (ruby)]. The rod was returned to Frankford Arsenal and re-aligned in the rangefinder.

## Bleaching Kinetics and Band Resolution

The basic problem in hardening the ruby laser, deduced from the relative fluorescent measurements, and demonstrated by the Frankford Arsenal test, is to reduce the radiation damage to the most vulnerable part of the system, which is the ruby rod. The principle permanent damage mechanism to the rod is color center formation in the ruby.

These color centers have been studied by a number of workers<sup>14-17</sup> and although several defect models have been proposed, none has been conclusively demonstrated. If the defect center can be identified to be a removeable impurity or defect structure, ruby can be made harder to nuclear radiation.

This phase of the experimental program at this laboratory was to investigate the color centers, determine their ultra-violet bleaching characteristics, and observe possible chromium losses due to irradiation. The bleaching experiments make possible the evaluation of the effectiveness of a flash lamp in optically annealing the radiation damage. The chromium loss is also shown to be an important defect mechanism in a irradiated laser.

Optical bleaching of the radiation produced coloration of materials has been successfully used with the alkali halides<sup>18,19</sup> to strengthen arguments for the defect models. Such bleaching experiments in ruby would hopefully yield further information on the radiation induced optical absorption.

Several authors<sup>14-17</sup> have agreed that there are several bands composing the additive absorption of irradiated ruby, but they have not agreed upon the

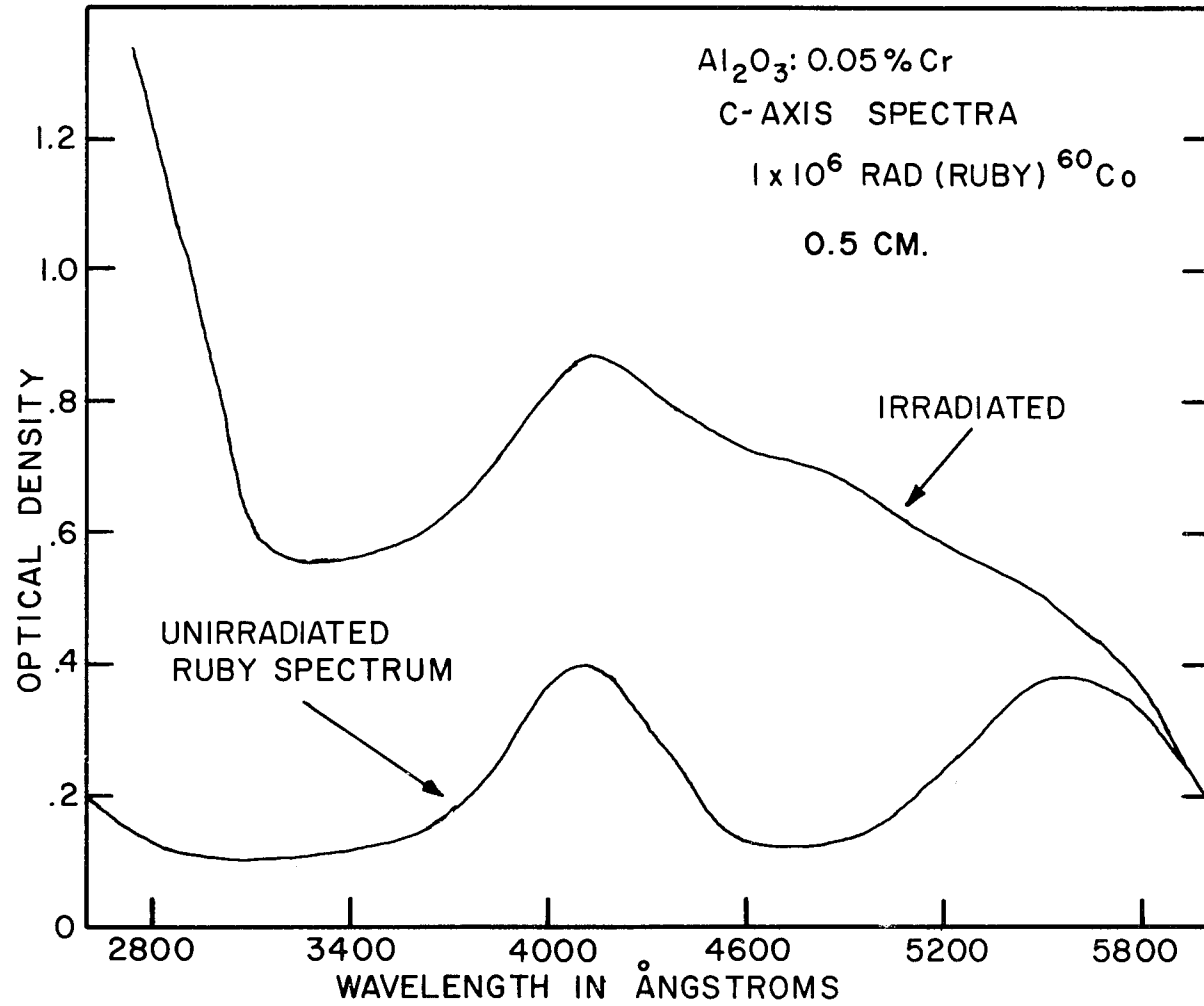


Fig. 13

UNIRRADIATED AND IRRADIATED RUBY ABSORPTION SPECTRUM

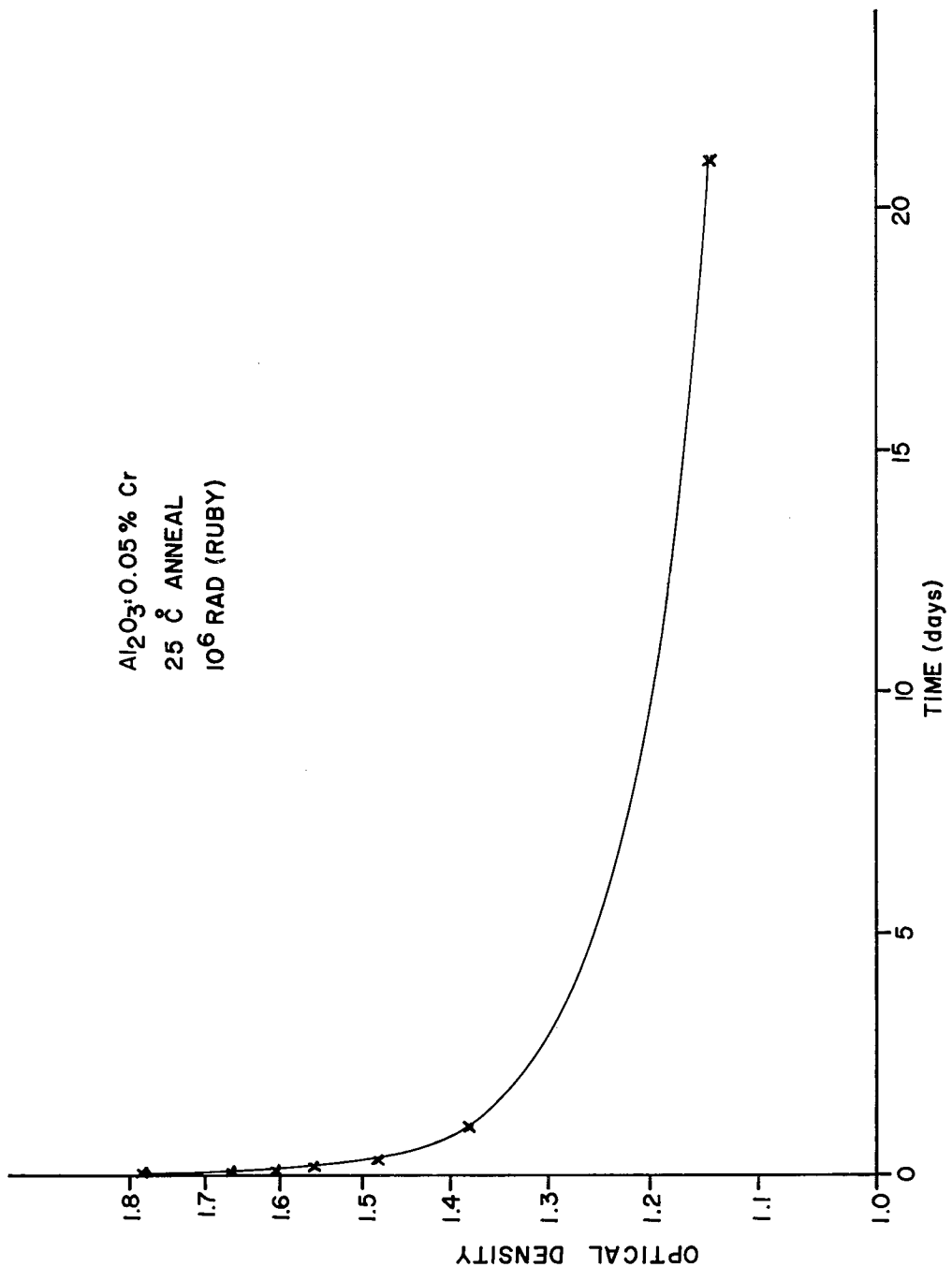


Fig. 15  
 ROOM TEMPERATURE ANNEAL FOR LONGER TIMES

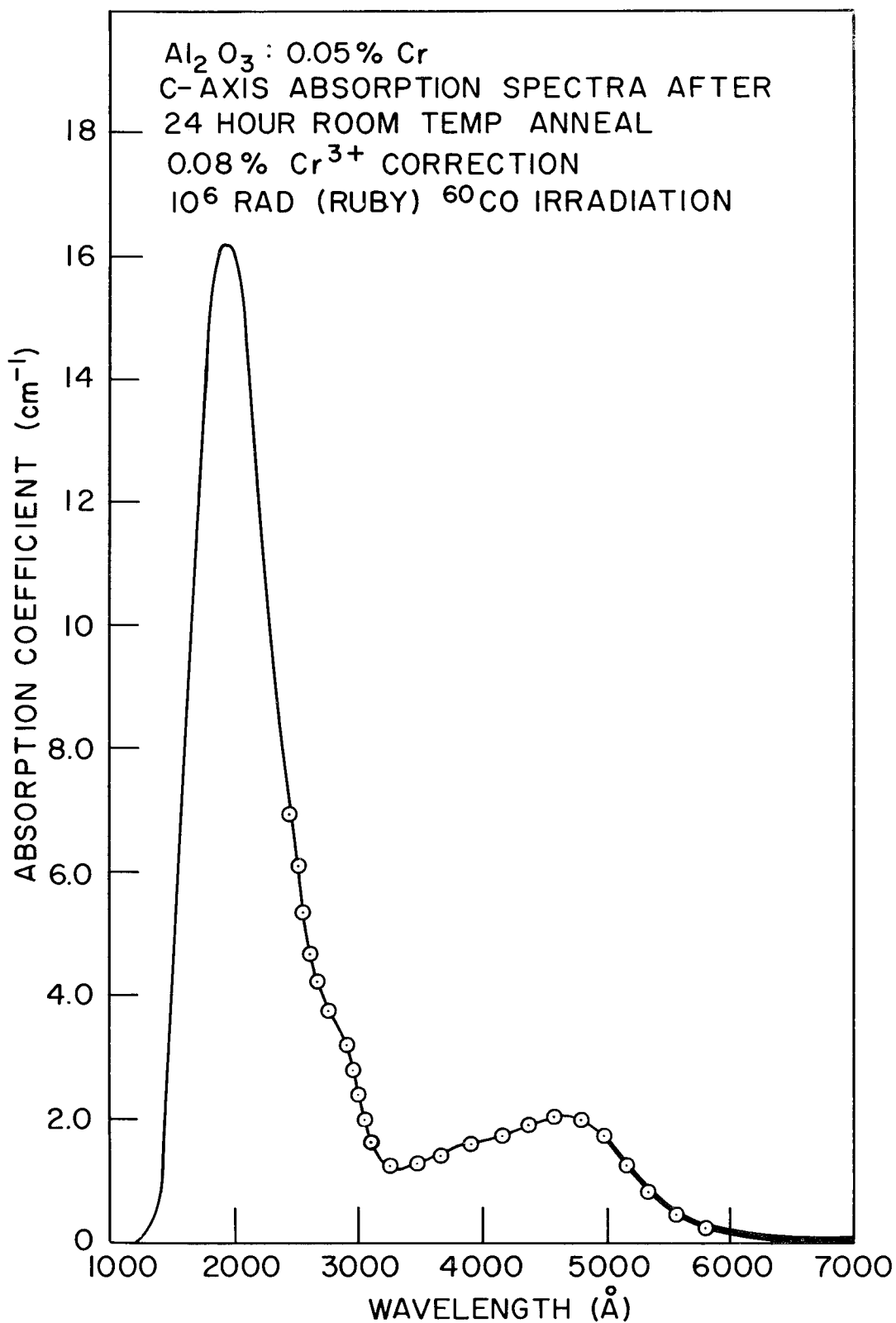


Fig. 16  
 ABSORPTION COEFFICIENT OF THE INDUCED ABSORPTION  
 The experimental data is indicated by the circles.

of bands was varied from 3 to 6. The best correlation occurs for four bands. However, for even the best fit to the data there was always an unaccounted for residual at about 5500Å.

A possible cause of this residual was a change in the  $\text{Cr}^{3+}$  concentration. In that case, the underlying  $\text{Cr}^{3+}$  absorption bands would have decreased. Maruyama and Matsuda<sup>14</sup> (M&M) reported a sizeable (10 to 50%)  $\text{Cr}^{3+}$  ion decrease, which was observed by an electron paramagnetic resonance (EPR) experiment. EPR measurements at this laboratory (see page 58) confirmed a  $\text{Cr}^{3+}$  loss, but not to the magnitude M&M reported. To check the EPR results a measurement was made of the change in the total area of the optical absorption of the  ${}^2\text{E}$  levels (R lines, 6943 and 6928Å). The R lines were chosen because they were beyond the principle radiation induced absorption, their shape was unchanged by the irradiation, and the area under these absorption lines is proportional to the  $\text{Cr}^{3+}$  concentration.

The experimental procedure followed was to irradiate the crystal to  $1 \times 10^6$  rad (ruby)  ${}^{60}\text{Co}$ , place the sample in the Cary 14 spectrophotometer, and record the absorption spectra. After the optical bleach or room temperature anneal, another absorption measurement was made without moving the sample. Figure 17 shows the difference in the two spectra for a 0.05%  $\text{Cr}^{3+}$  crystal. It was found that optical bleaching using a mercury arc completely bleached the irradiation produced absorption. Because of color centers induced by the irradiation in the region of the R lines, (see page 29) the base line is raised. However, since the absorption is so broad, the

base line is relatively flat over a 100 Å region of interest. Also, the irradiation apparently shifts the R lines to higher energies, but does not broaden them. A planimeter was used to measure the area under each curve. The base lines for the curves were drawn from the flat region around 6900Å to the flat region around 6980Å.

This technique was used for several bleach and anneal cycles, yielding a  $\text{Cr}^{3+}$  concentration change of  $8 \pm 2\%$  for a saturating dose of  $1 \times 10^6$  rad (ruby)  $^{60}\text{Co}$ . This change is in good agreement with the EPR measurements ( $\sim 10\%$  decrease) which will be discussed on page 61.

It should be emphasized at this point that this measurement does not indicate that the  $\text{Cr}^{3+}$  changes into another element, but only that its charge state is changed by irradiation.

These studies reveal two significant facts: four Gaussian bands compose the radiation induced absorption spectra, and the  $\text{Cr}^{3+}$  concentration changes by about 8% for a 0.05% ruby crystal (laser grade and concentration) when irradiated with  $1 \times 10^6$  rad (ruby)  $^{60}\text{Co}$ . Taking the decrease in  $\text{Cr}^{3+}$  into account, the absorption data was re-analyzed by the GLSWS program. This fit is shown as the solid line in Fig. 16. To see how the component bands overlap one another, the computer was programmed to plot the bands, as shown in Fig. 18. Table II lists the parameters of the bands for this experimental data.

TABLE II

The Calculated Absorption Band Characteristics for  $\text{Al}_2\text{O}_3:0.05\% \text{Cr}^{3+}$ , Irradiated with  $10^6$  rad (ruby) and corrected for  $\text{Cr}^{3+}$  loss\*

Band Number	$\alpha$ ( $\text{cm}^{-1}$ )	$\Delta E$ (e V)	$E_0$ (e V)	$\lambda_0$ ( $\text{\AA}$ )
1	1.29	0.251	2.59	4790
2	1.44	0.497	3.12	3970
3	1.17	0.212	4.30	2880
4	16.2	1.27	6.48	1914

\*The spectra were taken with the light directed along the c axis ( $E \perp c$ ).

This calculation was made on the data from two other independent experimental runs under differing bleaching conditions, for the 0.05%  $\text{Cr}^{3+}$  crystal. The amplitudes of the absorption coefficients will vary, depending on the experimental conditions. However, the values of  $E$ ,  $\Delta E$ , and  $\lambda$  should not change if the resolution is correct. The values of  $\Delta E$ ,  $E$ , and  $\lambda$  for these runs are listed along with their average values in Table III.

To understand the restriction of  $\Delta\alpha$ , consider the rate equation:

$$\frac{dn}{dt} = -\sigma I n^i \quad (2)$$

where

$n$  - number of defects/cc,

$\sigma$  - cross section of photon absorption,

$i$  - an integer which is a function of the order of the reaction,

$I$  - intensity of the bleaching light at any position in the crystal  
and at any time  $t$ .

The intensity of the light,  $I$  varies over the thickness of the crystal.

$$I = I_0 \exp [ -(\alpha_c + \alpha_d(t)) x ] \quad (3)$$

where

$I_0$  - intensity at  $t = 0$  and at  $x = 0$

$\alpha_c$  - absorption coefficient of the  $\text{Cr}^{3+}$  ion at the wavelength  
( $\lambda_b$ ) of the bleaching light.

$\alpha_d$  - absorption coefficient of the defect at  $\lambda_b$

$x$  - distance in the crystal measured along the direction  
of the bleach light.

If  $I$  is strongly dependent on  $t$ , then Eq. (2) is difficult to solve. But if the dependence on  $t$  is weak, the solution of Eq. (2) is considerably simplified. Experimentally, the intensity  $I$  can be made approximately constant in time if  $\alpha_d$  is small compared with  $\alpha_c$ . For this reason the bleaching wavelength,  $\lambda_b$  should be on the tail of the induced absorption

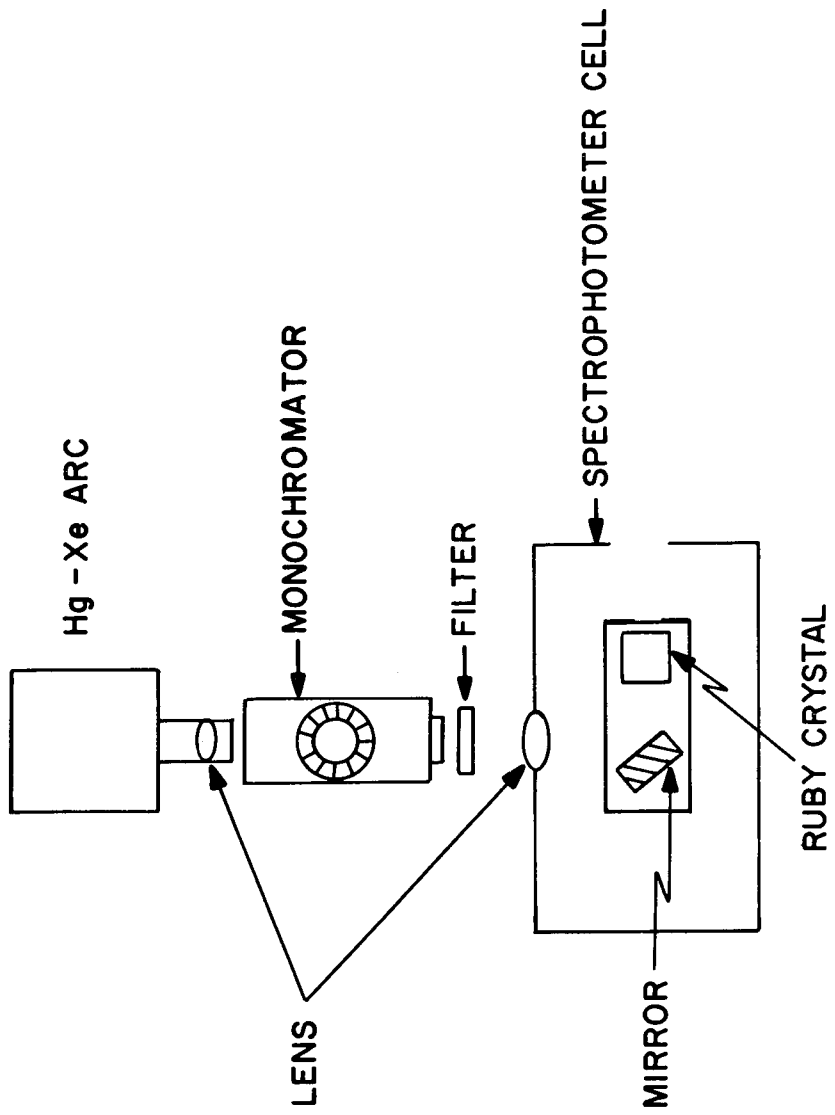


Fig. 19

SCHEMATIC OF BLEACHING APPARATUS

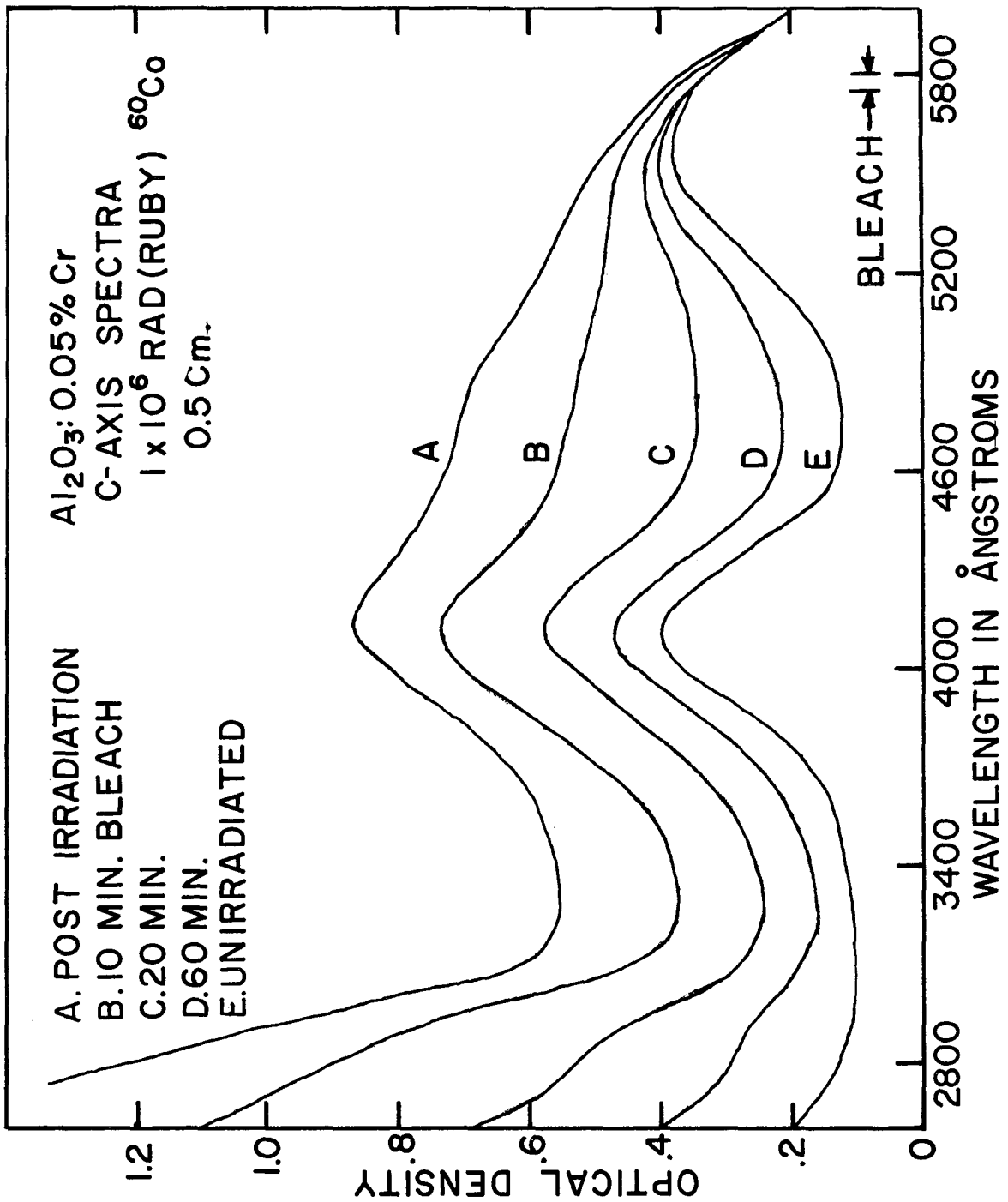


Fig. 20

IRRADIATED RUBY ABSORPTION SPECTRA

The absorption spectrum of ruby is shown after irradiation and after several bleaching intervals. The bleaching wavelength is at 5800 Å.

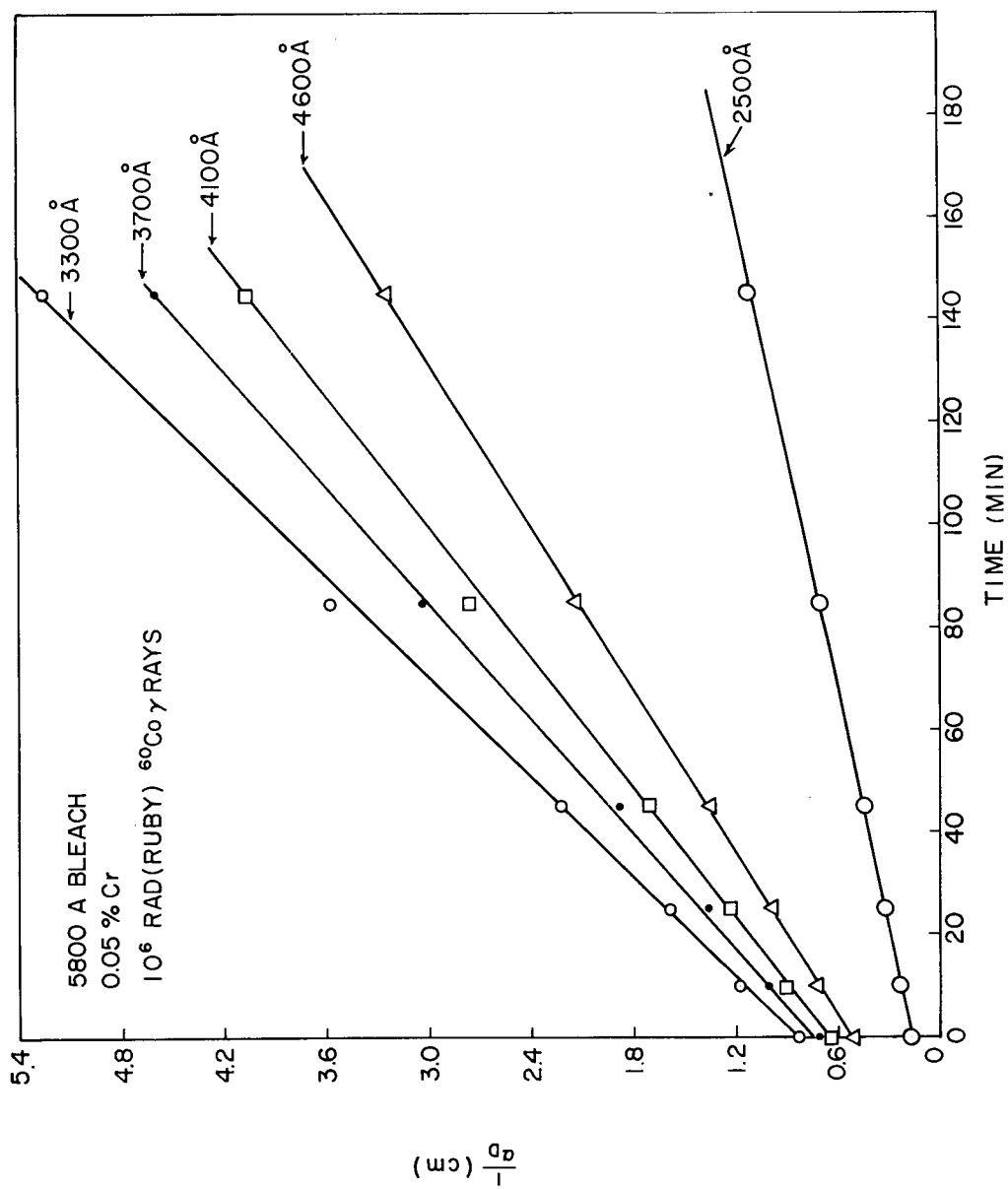


Fig. 21

INVERSE ABSORPTION COEFFICIENT VERSUS BLEACHING TIME

magnetic field of interest, the number obtained is proportional to the number of  $\text{Cr}^{3+}$  ions.

The actual shape of the EPR derivative trace can vary considerably. However, for dilute unirradiated, low concentration ruby, ( $\text{Cr}^{3+} \leq 0.01\%$ ), the absorption is known to have a Gaussian lineshape<sup>24</sup>. For a Gaussian lineshape only, the area under the absorption curve is proportional to  $(\Delta H)^2 \cdot \Delta P$ , where  $\Delta H$  is the peak to peak width of the derivative trace, and  $\Delta P$  is the peak to peak height of the derivative trace. If  $\Delta H$  does not change as the crystal is irradiated, the number of  $\text{Cr}^{3+}$  ions is proportional to  $\Delta P$ . Figure 22 shows a typical derivative trace, with  $\Delta H$  and  $\Delta P$  labeled.

If the EPR absorption signal of the  $\text{Cr}^{3+}$  ions is obtained with the magnetic field directed along the crystallographic c axis of the sample, called the parallel orientation, three  $\text{Cr}^{3+}$  resonances can be observed. One of the resonances, labeled  $1/2 \rightarrow -1/2$  for the spin quantum numbers of the energy levels between which the EPR transition takes place, is ideal for the observation of  $\text{Cr}^{3+}$  changes by irradiation because it is not affected by strains and electric fields which might be caused by radiation induced defects<sup>2</sup>.

The same crystal used for the optical absorption measurement (0.05%  $\text{Cr}^{3+}$ ) was irradiated to  $1 \times 10^6$  rad (ruby) <sup>60</sup>Co. The EPR signal of the  $1/2 \rightarrow -1/2$  transition was measured in the parallel orientation. Without removing or handling the sample, the color centers were bleached from the sample by a Hanovia Hg arc (230 watts). The EPR signal was taken again after the crystal had been completely bleached.

In comparing the pre and post bleach EPR data, it was found that the shape and peak to peak width ( $\Delta H$ ) remained the same, but that the peak to peak height ( $\Delta P$ ) decreased by  $12 \pm 2\%$ . This indicates a decrease in the  $\text{Cr}^{3+}$  concentration of  $12 \pm 2\%$ , and agrees well with the  $\text{Cr}^{3+}$  loss on irradiation for this sample obtained by optical means ( $8 \pm 2\%$ ).

The other two EPR transitions observed in the parallel orientation are designated  $3/2 \rightarrow 1/2$  HF, LF, respectively. The transitions take place between the same two spin levels, but the first occurs at about 750 gauss (LF = low field), and the second at 7500 gauss (HF = high field) for an X-band spectrometer. Only the first is observable with the Varian E-3 spectrometer used for these experiments because of magnetic field limitations, but either transition gives the same information.

In contrast to the  $1/2 \rightarrow -1/2$  transition, the  $3/2 \rightarrow 1/2$  transitions are affected by electric fields. (Strain field effects are not expected since these are associated with displacement damage which was negligible in this case.) When a uniform electric field is applied to a ruby crystal, the  $3/2 \rightarrow 1/2$  EPR transitions are observed to shift in resonant magnetic field.<sup>25</sup> The formerly single line splits into two components, which shift symmetrically on either side of the zero electric field line. The magnitude of the shift versus electric field in ruby is given by<sup>25</sup>

$$\Delta H = \pm A E_z, \quad (7)$$

for this transition at  $\theta = 0^\circ$ , where A is  $0.194 \text{ gauss cm}(\text{KV})^{-1}$ , and only the z component of the electric field,  $E_z$ , is effective in shifting the EPR line.

broadening mechanisms are independent, and the resultant lineshape is the convolution, or folding, of one lineshape into the other:

$$F(H) = \int_{-\infty}^{+\infty} I(H') \cdot G(H - H') dH' \quad (10)$$

where  $G(H)$  is the pre-irradiation lineshape. It is this lineshape that must be compared with the experimental data to obtain  $n$ .

Irradiations and EPR measurements were carried out on a series of rubies of varying  $\text{Cr}^{3+}$  concentration. The  $3/2 \rightarrow 1/2$  transition was observed before and after the irradiation, and the linewidth and the lineshape were observed to drastically change.

The change in lineshape probably accounts for the anomalously large loss of  $\text{Cr}^{3+}$  ions reported by MandM<sup>14</sup>. If the lineshape is not Gaussian, simply taking  $(\Delta H)^2 \cdot \Delta P$  as proportional to the number of  $\text{Cr}^{3+}$  ions is not correct.

The lineshape, given by Eqs. (8) and (10) was fitted to the post-irradiation shape using  $n$  as an adjustable parameter. Figure 23 shows the best fit for a sample of 0.0103%  $\text{Cr}^{3+}$  Verneuil ruby, after a saturating dose of  $^{60}\text{Co}$  gamma rays. The pre-irradiation lineshape is shown on the figure (not to scale). The best fit was obtained for a charged defect density of  $2.3 \times 10^{17}$  per  $\text{cm}^3$  charges of either sign. The very good fit to a single parameter theory gives confidence in this method. The estimated error in  $n$  was about  $\pm 20\%$ . This error is due mostly to uncertainty in the constants  $A$  in Eq. (9).

The experiment was also performed on the sample used in the previous EPR experiment and in the optical experiments (.05% Cr<sup>3+</sup>). Figure 24 shows the derivative EPR trace of the 3/2 → 1/2 transition (1) after irradiation, and (2) after the induced optical absorption has been bleached. Curve (3) is curve (1) normalized to curve (2). The best fit is obtained for a charged defect concentration of  $(6 \pm 1.5) \times 10^{17} / \text{cm}^3$ . The fit (not shown) is not entirely satisfactory in the wings of the line. This will be discussed on page 67.

A series of experiments of this type have been performed on nine crystals of varying Cr<sup>3+</sup> concentration and of different growth types, both Czochralski and Verneuil. These samples were exposed to a saturation dose of <sup>60</sup>Co gamma rays, and the EPR lineshape fitted to obtain n. Also, the 1/2 → -1/2 transition was observed, and the number of Cr<sup>3+</sup> which change valence state are also simultaneously obtained. The results of this study are shown in Table VI.

TABLE VI

Charged defect density  $n$ , observed  $\text{Cr}^{3+}$  loss, and optical absorption coefficient at  $4790\text{\AA}$  for nine rubies. V and Cz signify Verneuil and Czochralski growth methods, respectively.

Sample Number and Type	$\text{Cr}^{3+}$ Concentration in percent	$n$ in $10^{17}/\text{cm}^3$	$\text{Cr}^{3+}$ loss in percent	$\text{Cr}^{3+}$ loss in $10^{17}/\text{cm}^3$	Absorption Coefficient in $\text{cm}^{-1}$
1 V	0.0008	---	15.7	0.59	0*
2 Cz	0.003	0.62	14.3	1.4	0.40
3 Cz	0.0093	2.0	10.6	3.1	0.57
4 V	0.0103	2.3	10.7	3.4	0.75
5 Cz	0.0101	2.0	10.8	3.4	----
6 V	0.026	3.2	8.7	7.1	0.93
7 Cz	0.054	6.9(5.1)**	9.3	16.0	2.13
8 Cz	0.058	5.9	12.0	20.0	----
9 V	0.10	6.9	----	---	2.4

\*The optical absorption of the 0.0008% Cr sample is due to the set of color centers which form in very low concentration ruby (sapphire).<sup>9</sup> This optical absorption ( $0.12 \text{ cm}^{-1}$ ) has been subtracted from all the other absorption coefficients.

\*\*The data from sample 7 has been analyzed in terms of an isolated defect density  $n$  only, and also in terms of an additional dipole defect density. The value of  $n$  in the latter case is shown in parenthesis. See page 69.

The estimated errors in the above data are  $\pm 20\%$  for the  $\text{Cr}^{3+}$  loss and  $n$ ,  $\pm 20\%$  on the  $\text{Cr}^{3+}$  concentration, and  $\pm 5\%$  on the optical absorption coefficient.

$$I(H) = B/[H^2 + (\Gamma/2)^2] \quad (11)$$

where B is a normalization constant, and

$$\Gamma = 2/3 (n_d P_z) \cdot A \cdot \pi / (\epsilon_0 \epsilon_z) \quad (12)$$

where  $n_d$  is the number of dipoles/cm<sup>3</sup>,  $P_z$  is the z component of the electric dipole moment (MKS) and A,  $\epsilon_0$  and  $\epsilon_z$  were defined in Eq. (9).

The broadening given by Eq. (12) would also be independent of the hyperfine and isolated charged defect broadening. The resulting lineshape would be a convolution of Eq. (10) with Eq. (11). The data from the 0.054% Cz sample, shown in Fig. (24) was analyzed on the basis of this additional source of broadening, varying both n and  $\Gamma$ .

Figure (25) shows the fit to the data. The solid line is the experimental data and the x indicate the theoretical fit. Very good agreement can be obtained. This fitting resulted in a  $\Gamma$  of 2.5 gauss, for which  $(n_d P_z) = 6.15 \times 10^{-5}$  coul/m<sup>2</sup>. in this example  $n = 5.1 \times 10^{17}$ /cm<sup>3</sup>.

In this case, the product of the dipole defect density and the z component of the electric dipole moment is determined. Since the structure of the dipole defect is not known, the dipole moment is also unknown. The most simple type of defect would be a Cr<sup>4+</sup> or Cr<sup>2+</sup> ion in one Al location of the Al<sub>2</sub>O<sub>3</sub> molecule with the charge compensating defect in the other Al site of the Al<sub>2</sub>O<sub>3</sub> molecule. The distance between these sites is 2.73 Å and the ions are aligned along the z axis.

The dipole moment would then be  $e \cdot 2.73 \times 10^{-8}$  Coulomb meters. This neglects possible polarization effects in the immediate surroundings of the ion which are undoubtedly present and which would tend to reduce the dipole moment. However, choosing this value for the dipole moment should provide an order of magnitude estimate of the dipole concentration.

The dipole concentration calculated from Eq. (12) using this value is

$$n_d = 1.3 \times 10^{18} / \text{cm}^3$$

Referring to Table VI, Sample 7, the total  $\text{Cr}^{3+}$  loss is  $1.6 \times 10^{18} / \text{cm}^3$ , and one half of  $0.51 \times 10^{18}$ , or  $0.26 \times 10^{18}$  of the isolated defects (n) can be attributed to Cr in a valence state other than  $3+$ . The dipole concentration, which also involves Cr in different valence states, is  $1.3 \times 10^{18} / \text{cm}^3$ . Thus with this simplified model for the dipoles, the chromium loss can be accounted for. However, in view of the very simple model employed for the dipole concentration, the good numerical agreement must be considered as fortuitous pending further experiments. The dipole model must then be considered as tentative.

Thus two distinct types of defects appear to be observed in irradiated ruby. The dipole defects account for most (80%) of the  $\text{Cr}^{3+}$  loss, one of the two detrimental effects of irradiation on a ruby laser.\*

The second effect, color center formation, can be associated with the isolated charged defects. Figure (26) shows the radiation saturated optical absorption of the radiation induced color centers, taken at  $4790 \text{ \AA}$ , plotted against the number of isolated charged defects. This data is taken from Table VI, page 67

---

\*The results of this study will be submitted for publication.

The data indicates that the dependence is linear. Note that the  $\text{Cr}^{3+}$  concentration varies over a factor of about 30. Thus the color centers are well correlated with the isolated charged defect density. The absorption coefficient per color center, calculated from Fig. 26, is then  $3 \times 10^{-18} \text{ cm}^2$ .

Figure (27) shows the absorption coefficient of the color centers plotted against the  $\text{Cr}^{3+}$  concentration remaining in the sample after irradiation, on a log-log scale.

The slope of the line indicates a dependence of the color center concentration on the  $\text{Cr}^{3+}$  concentration remaining in the crystal of about

$$[ \text{Color centers} ] = K \cdot [ \text{Cr}^{3+} ]^{0.6}. \quad (13)$$

This compares favorably with the results of M&M<sup>14</sup>

$$[ \text{Color centers} ] = K \cdot [ \text{Cr}^{3+} ]^{0.55}. \quad (14)$$

This relation will be useful in determining a model for the color center defect which will be discussed in the next section.

The data given in Table VI also indicates that the amount of  $\text{Cr}^{3+}$  lost by irradiation is about 10% of the  $\text{Cr}^{3+}$  concentration, independent of the  $\text{Cr}^{3+}$  concentration.

### Defect Model

Based on the kinetic studies, the EPR measurements and the color center optical absorption, a tentative model for the defects which affect laser action can be proposed.

The EPR data indicate two types of defects; an isolated charged defect and a dipole-like defect.

The number of isolated charged defects is much smaller than the observed  $\text{Cr}^{3+}$  loss. These defects are but a small fraction of the total number of radiation induced defects. However, the defect absorption ( $\alpha_d$ ) is correlated with the number of isolated charged defects. It is therefore reasonable to ascribe the color centers to the isolated charged defects, or to the chromium ions in another valence state which are associated with the isolated charged defects.

The dependence of the color center concentration on the  $\text{Cr}^{3+}$  content is close to

$$[\text{Color centers}] = K \cdot [\text{Cr}^{3+}]^{0.5}. \quad (15)$$

When a radiation process shows saturation, i. e., no increase in concentration with increasing dose, the process is in equilibrium in that the process and the radiation-induced back reaction results in equal rates in both directions. This is very similar to chemical equilibrium and many of the chemical concepts can be carried over. If the formation reaction for the defect were



or



then in equilibrium (or saturation) where the concentrations do not change with increasing dose, the reasoning leading to the chemical mass-action

Such an equation could also hold for other valence states of Cr. However, other charged states of Cr are not as likely, since the charge states that result are usually less stable ( $\text{Cr}^{5+}$  and  $\text{Cr}^{1+}$ ). The other possible charge state is given by the reaction



This state is also unlikely since such highly charged defects are in general not observed in radiation damage in insulators. Thus it is probable that the defects are singly charged, and one of the Equations (16) is the defect reaction for the isolated charged defect.

It is also unlikely that the induced absorption is associated with the  $\text{Cr}^{2+}$  and  $\text{Cr}^{4+}$  ions. Since the number of the defects and their absorption coefficient is known, the absorption cross section is also known. The absorption cross section of an individual color center is about  $3 \times 10^{-18} \text{ cm}^2$ . This is to be compared with the cross sections which are typical of the other 3d transition ions in solids,  $2 \times 10^{-19} \text{ cm}^2$  ( $\text{Cr}^{3+}$  in  $\text{Al}_2\text{O}_3$  for the pump bands). About the same order of magnitude cross section are expected of  $\text{Cr}^{2+}$  and  $\text{Cr}^{4+}$ . Thus the observed absorption cross section is about an order of magnitude too large to be associated with the chromium ion. The induced absorption then appears to be associated with  $\text{D}^-$ , or  $\text{D}^+$  defect.

Since the optical defect shows four bands which all optically bleach when any one band is optically bleached, it is likely that the defect is associated with an impurity ion complex, because in F or V type optical centers, (holes or electrons trapped at a vacancy) as observed in

## Increase in Ruby Laser Output by $^{60}\text{Co}$ Irradiation

Increases in ruby laser output after  $^{60}\text{Co}$  irradiation have been observed by several investigators.<sup>31-33</sup> Output increases by factors of two and three have been observed for  $^{60}\text{Co}$  exposures of  $1 \times 10^3$  to  $6 \times 10^3$  R.<sup>33</sup> The increase in laser output has been observed, however, only when the laser is pumped at greater than twice threshold. These effects were not considered in this work as no military ruby laser system is operated so high above threshold. Some comments are in order since information on this effect can be gained from the preceding discussion. Two mechanisms are proposed for the increased laser output at high pumping levels.

The first mechanism is that at high flash lamp intensities, very efficient optical bleaching of the color centers takes place. This bleaching releases electrons (or holes) which recombine with holes (electrons) at the chromium ion. This leaves the  $\text{Cr}^{3+}$  ion in an excited state which decays very quickly to the R levels, thus increasing the R level population. This would lead to an increased laser output.

The maximum possible increase in laser output for a  $0.05 \text{ Cr}^{3+}$  ruby laser rod can be calculated since the number of color centers is known. The maximum number of charged defects  $n$ , which is twice the number of color centers, is about  $5 \times 10^{17}/\text{cm}^3$  for a  $1 \times 10^6$  rad (ruby irradiation). If each color center is associated with a chromium ion in a valence state other than  $3+$ , and when bleached produces one excited  $\text{Cr}^{3+}$  ion, the resulting maximum laser output would be  $2.5 \times 10^{17}$  photons/ $\text{cm}^3 \times 1.8$  eV photon  $\times 1.6 \times 10^{-19}$  joule/eV =  $0.07$  joule/ $\text{cm}^3$ .

TABLE VII

Damage Parameters in Linde 0.05% Czochralski Ruby Irradiated to  $10^4$  Rads

$\text{Cr}^{3+}$  Loss - Less than 3%

Induced Optical Density at R line -  $0.002 \text{ cm}^{-1}$

Induced Optical Density at  $4790\text{\AA}$  (E  $\perp$  C)  $0.65 \text{ cm}^{-1}$

(E  $\parallel$  C)  $0.37 \text{ cm}^{-1}$

Two values are given for the absorption coefficient at  $4790\text{\AA}$  since the absorption is different if the electric vector is parallel, (E  $\parallel$  C) or perpendicular, (E  $\perp$  C), to the crystallographic c-axis of ruby. The ratio of the two values (1.75) is a fixed constant for the defect absorption. The band at  $2880\text{\AA}$  is also anisotropic with the ratio of 1.2 for the E  $\perp$  C/E  $\parallel$  C absorption coefficients.<sup>14</sup> The other bands do not exhibit directional effects. The band location, widths, and ratio of the component amplitudes will be the same as those given in Table II on page 48. The magnitude of the induced absorptions is thus fixed by the single value of the absorption measured in the E  $\perp$  C direction for  $4790\text{\AA}$ . The laser output can be written as [the formula and definitions are taken from Ref. (12)],

$$E_{\text{out}} = N_o h\nu (t_{\text{pump}} - t_{\text{th}}) \cdot V [WN_1(t_{\text{th}}) / \{N_o - N_2(t_{\text{th}}) / \uparrow N_o\}] \cdot [ |\ln r_1 r_2| / |\ln r_1 r_2 + 2 \beta L| ] \quad (21)$$

where

$N_o$  =  $\text{Cr}^{3+}$  density,  $\text{cm}^{-3}$

V = lasing volume of the ruby rod

$t_{\text{pump}}$  = duration of pumping pulse

For an irradiation of  $1 \times 10^4$  rads,  $N_0$  decreases by less than 3%.

From the value of  $N_1$  at threshold, the threshold increases by less than 3% and, since  $N_1$  and  $N_2$  depend on  $N_0$ , the power output at any level decreases by less than 3%, which is negligible. The radiation induced absorption at the R line is  $0.002 \text{ cm}^{-1}$ . This absorption acts like the scattering loss,  $\beta$ , and can be combined with it. A typical range of values for the scattering loss<sup>29</sup> in ruby is  $0.025$  to  $0.05 \text{ cm}^{-1}$ . The R line absorption is thus negligible when compared with the scattering loss.

The light absorbed by the defects, and consequently not by the  $\text{Cr}^{3+}$  ions, is sizeable. This is the principle damage mechanism at  $1 \times 10^4$  rads. This causes a reduction in  $T$ , the transmission of pump light, and thus of  $W$ , the pump rate.  $N_2$  in Eq. (21) is implicitly a function of  $W$ , so that to a first approximation, the power output is proportional to the pumping rate. The change in  $T$  by irradiation can be expressed as the ratio of the pump light intensity absorbed by the  $\text{Cr}^{3+}$ , before and after the irradiation.

The light intensity absorbed by the  $\text{Cr}^{3+}$  ions before irradiation is proportional to

$$1 - \exp(-\alpha_1 L) \quad (24)$$

where  $\alpha_1$  is the absorption coefficient of the  $\text{Cr}^{3+}$  pump bands and is a strong function of wavelength, and  $L$  is the width of the sample. The light intensity absorbed after the irradiation is proportional to

$$1 - \exp[-(\alpha_1 + \alpha_2) L] \quad (25)$$

where  $\alpha_2$  is the absorption coefficient of the induced color centers and is also a function of wavelength.

absorption coefficient are

$$\begin{aligned}\alpha_{\text{eff}} &= 0.5 \alpha_{\parallel} + 0.5 \alpha_{\perp} \quad (0^{\circ} \text{ rod}) \\ \alpha_{\text{eff}} &= 0.25 \alpha_{\parallel} + 0.75 \alpha_{\perp} \quad (90^{\circ} \text{ rod}) \\ \alpha_{\text{eff}} &= 7/16 \alpha_{\parallel} + 9/16 \alpha_{\perp} \quad (60^{\circ} \text{ rod})\end{aligned}\tag{28}$$

where  $\alpha_{\parallel}$  and  $\alpha_{\perp}$  are the  $E \parallel C$ ,  $E \perp C$  absorption coefficients, respectively, and  $0^{\circ}$ ,  $90^{\circ}$ ,  $60^{\circ}$  identifies the angle the c-axis makes with the axis of the laser rod. Since most laser grade ruby is grown in the  $60^{\circ}$  configuration, this will be used for the calculation.

The diameter of the rod (L) in Eq. (27) will be taken as 1/4 inch, a common rod diameter. The data is taken for convenience from spectrophotometer traces for a 0.05% linde ruby (irradiated to  $1 \times 10^4$  rad (ruby)).

The reduction of flashlamp intensity absorbed by the  $\text{Cr}^{3+}$ , calculated from Eq. (27) is 10%. This means that a laser operating at 110% threshold will cease lasing after an irradiation of  $1 \times 10^4$  rad.

At pumping levels above 110% threshold, the laser output will be reduced. The output reduction can be estimated by measuring the laser output as a function of the flash lamp intensity for the laser system. The post-irradiation output is then the output at a flashlamp intensity 10% less than the operating point. A sizeable reduction in laser output can occur for a 10% reduction in flashlamp intensity. For the laser system mentioned on page 3, operated at 700 joules (1.6 times threshold), the experimentally measured decrease in flashlamp intensity was 10% at  $1 \times 10^4$  rad, in very good agreement with the calculation. This 10% decrease in flashlamp energy

## V. SUMMARY

The mechanisms of ionizing radiation damage to a ruby laser are now fairly well understood. The transient cut-off of a long pulse ruby laser can be attributed to the formation of an ionized defect center composed of an  $O^-$  ion adjacent to a charge deficient cation site. This center produces an optical absorption centered at 3.08 eV (4000 Å) which is in the wings of the absorption line, overlapping the laser transition. This additional absorption depletes the coherent light inside the laser cavity below the threshold value, and the laser output ceases. Lasing resumes when the laser increases the population difference between the laser levels so as to overcome the absorption. This center is not completely stable at room temperature, and decays with a lifetime of about 10 m sec.

The permanent degradation effects of ionizing radiation on the ruby laser are caused by (1) the formation of four stable defect absorption bands which overlap the ruby pump bands, (2) a loss of  $Cr^{3+}$  by change of valence and (3) a permanent absorption at the R lines. The defect absorption competes with the  $Cr^{3+}$  ions for the pump light, thus decreasing the number of  $Cr^{3+}$  ions which can be made to lase at a given power input. The defect absorption is associated with change of valence state of the  $Cr^{3+}$  as it shows an explainable  $Cr^{3+}$  concentration dependence. This absorption does not appear to be associated with  $Cr^{2+}$ ,  $Cr^{4+}$  or  $Cr^{6+}$  since the absorption cross sections of the defects are too large. They are most likely caused by defects spatially remote from the  $Cr^{3+}$  ion which become ionized and provide charge compensation for part of the  $Cr^{3+}$  ions which have changed valence state.

then important to know which ions are responsible for the harmful defect centers. Some further work may be useful to identify the responsible ions.

The absorptions which overlaps the R line have been observed only recently and not much is known about their optical bleaching characteristics and their relation to the other absorption bands. It would be useful to investigate these defects in detail. Although the absorption is small at the lasing frequency, these defects have significant effect on the laser output at doses of  $1 \times 10^5$  rad or higher.

A worse case calculation of the effect of a dose of  $1 \times 10^4$  rads (ruby) shows that (1) the effect of the radiation induced optical absorption at the R line is negligible, (2) the chromium loss is less than 3% and negligible, and (3) the color center absorption in the pump bands reduces the pumping efficiency by 10% for any laser using a Linde 0.05% rod with a  $60^\circ$  orientation. Thus a ruby laser operating at 110% threshold would be shut off by a dose of  $1 \times 10^4$  rads. In experiments on a typical laser, a 10% reduction in the pumping efficiency resulted in a 30% output reduction. The radiation degradation effects are well enough known to permit the calculation of a worse case output reduction of a given system, given the parameters of the system and the dose.

22. J. J. Halpin, Bull. Am. Phys. Soc. 13, 1649 (1968).
23. W. E. Daniels Jr., Technical report No. 579, U. Of Maryland (1966).
24. W. J. C. Grant and M. W. P. Strandberg, Phys. Rev. 135, A724 (1964).
25. E. B. Royce and N. B. Bloembergen, Phys. Rev. 131, 1912 (1963).
26. W. B. Mims and R. Gillen, Phys. Rev. 148, 438 (1966).
27. A. M. Stoneham, Rev. Mod. Phys. 41, 82 (1969).
28. T. H. Maiman et al., Phys. Rev. 123, 1151 (1961).
29. A. K. Levine, Lasers Vol. 1, Marcel Dekker Inc., New York (1966) p. 33.
30. C. M. Stickley, Private communication.
31. W. Flowers and J. Jenny, Proc. IEEE 51, 858 (1963).
32. V. R. Johnson and R. W. Grow, IEEE, J. Quant. Elec., QE-3, 1 (1967).
33. W. R. Davis et al., J. A. P. 36, 670 (1965).
34. F. Varsanyi et al., Phys. Rev. Let. 3, 544 (1959).